Alpha-actinin binding kinetics modulate cellular dynamics and force generation

Allen J. Ehrlicher[a,b,c,1], Ramaswamy Krishnan[d], Ming Guo[b], Cécile M. Bidan[d], David A. Weitz[b], and Martin R. Pollak[a,1]

[a]Division of Nephrology, Department of Medicine, and [d]Department of Emergency Medicine, Beth Israel Deaconess Medical Center, Harvard Medical School, Boston, MA 02215; [b]School of Engineering and Applied Sciences, Harvard University, Cambridge, MA 02138; and [c]Department of Bioengineering, McGill University, Montreal, QC, Canada H3A0C3

Contributed by Martin R. Pollak, March 25, 2015 (sent for review January 14, 2015)

The actin cytoskeleton is a key element of cell structure and movement whose properties are determined by a host of accessory proteins. Actin cross-linking proteins create a connected network from individual actin filaments, and though the mechanical effects of cross-linker binding affinity on actin networks have been investigated in reconstituted systems, their impact on cellular forces is unknown. Here we show that the binding affinity of the actin cross-linker α-actinin 4 (ACTN4) in cells modulates cytoplasmic mobility, cellular movement, and traction forces. Using fluorescence recovery after photobleaching, we show that an ACTN4 mutation that causes human kidney disease roughly triples the wild-type binding affinity of ACTN4 to F-actin in cells, increasing the dissociation time from 29 ± 13 to 86 ± 29 s. This increased affinity creates a less dynamic cytoplasm, as demonstrated by reduced intracellular microsphere movement, and an approximate halving of cell speed. Surprisingly, these less motile cells generate larger forces. Using traction force microscopy, we show that increased binding affinity of ACTN4 increases the average contractile stress (from 1.8 ± 0.7 to 4.7 ± 0.5 kPa), and the average strain energy (0.4 ± 0.2 to 2.1 ± 0.4 pJ). We speculate that these changes may be explained by an increased solid-like nature of the cytoskeleton, where myosin activity is more partitioned into tension and less is dissipated through filament sliding. These findings demonstrate the impact of cross-linker point mutations on cell dynamics and forces, and suggest mechanisms by which such physical defects lead to human disease.

Alpha-actinin | actin | kidney disease | cell mechanics | traction force

Movement, morphology, and force production are essential aspects of animal life. At the cellular level, these mechanics are largely determined by the actin cytoskeleton—a network of actin filaments connected by cross-linkers to create a 3D biopolymer frame. These cross-linkers are not permanent, but bind transiently. Studies using reconstituted proteins show that when these cross-linkers are attached to and connect multiple filaments, they create a network that behaves like a weak elastic solid. When cross-links unbind, actin filaments are free to slide past one another, producing a network that behaves more like a viscous fluid (1, 2). This dynamic cross-linking makes the actin network a viscoelastic material that is solid-like on short timescales such as seconds, yet fluid-like on longer timescales such as minutes (3, 4).

The timescale of the transition from solid to fluid-like behavior in reconstituted actin networks is set by the duration of cross-linking, which is in turn set by cross-linker dissociation rate, K_{off} (1, 5, 6). The ability for an actin network to move between solid and fluid-like states may be an essential mechanism to balance mechanical and structural integrity of an elastic solid with adaptability and movement (1, 7–9). Despite this clear physical role of actin cross-linking in reconstituted network mechanics, the impact of changes in cross-linker affinity on cell force generation has not, to our knowledge, been previously investigated.

To examine the role of cross-linking dynamics on cellular forces, we study α-actinin, a 100-kDa actin cross-linking protein that exists as a dumbbell-shaped head-to-tail homodimer of ∼40 nm (10). α-Actinin binds to actin using two N-terminal calponin homology regions, which together create actin-binding domains (ABDs). These domains on opposite ends of the dimer allow α-actinin to act as a cross-linker, forming networks of loose bundles of actin filaments (11, 12). In humans, there are four genes that encode highly homologous forms of α-actinin. Point mutations in the ABD of ACTN4 cause a form of kidney damage known as focal segmental glomerulosclerosis (FSGS) (13–15). With FSGS, the specialized podocyte cells that form part of the filtration barrier between the blood and urine lose their normal extended structure (13). This dysfunction leads to malfunction of the glomerular filter and decreased renal function that often progresses to kidney failure (15). In particular, one point mutation (K255E) appears to expose a cryptic actin-binding site, which increases the affinity of ACTN4 for actin. Previous research using purified proteins has shown that this K255E mutation creates a more elastic and solid-like actin network (6, 16–18). Because the moduli of reconstituted actin networks are highly sensitive to cross-linker affinity and concentration (1, 2, 19), we hypothesized that changes in actin cross-linking will also significantly impact the total force and work exerted by an active cell on its environment. However, the effect of this mutation, or variable cross-linking in general, on the dynamics and forces of cells is largely unknown (20). Understanding how cross-linker binder affinity changes force generation will provide essential insight into how cells modulate their mechanics, and exert forces on their surrounding environment.

In this article we quantify the affinity of variable ACTN4 cross-linking and its effects on cellular movement, intracellular transport, and traction forces. We measure that the K255E mutant form of

Significance

In this study, we examine how proteins that cross-link actin filaments control certain biophysical aspects of living cells. We studied α-actinin-4 (ACTN4) a dimeric rod-shaped homodimer, of particular interest because mutations in its actin binding domain cause a human disease characterized by dysfunction of the kidney's glomeruli; however, the mechanical impact of such mutations are unknown. We find that the human disease-causing K255E mutation in ACTN4 leads to a change in cellular biophysical properties, increasing the affinity for actin increases cellular forces and work, while decreasing cell movement. These observations describe the effects of variable cross-linking on cellular forces and dynamics, and reveal how pathology may arise mechanically from disruptive point mutations in cytoskeletal proteins.

Author contributions: A.J.E., R.K., and M.R.P. designed research; A.J.E., R.K., and M.G. performed research; A.J.E., R.K., D.A.W., and M.R.P. contributed new reagents/analytic tools; A.J.E. and C.M.B. analyzed data; and A.J.E., R.K., and M.R.P. wrote the paper.

The authors declare no conflict of interest.

See Commentary on page 6527.

[1]To whom correspondence may be addressed. Email: mpollak@bidmc.harvard.edu or allen.ehrlicher@gmail.com.

This article contains supporting information online at www.pnas.org/lookup/suppl/doi:10.1073/pnas.1505652112/-/DCSupplemental.

ACTN4 has a threefold increase in affinity for actin in cells compared with wild type. This increased affinity creates a cell that is ∼50% less motile and displays 70% less cytoplasmic mobility. Surprisingly, though this mutation reduces both intra- and extracellular movement, it increases contractile stresses by 300%, and the total work done on the substrate by 500%. Thus, this point-mutation change in cross-linker binding has profound macroscopic effects on cell dynamics and force translation, providing a sensitive mechanism for the cell to modulate myosin work between cell contractility and movement.

Results and Discussion

ACTN4 Binding-Site Mutations Change Its Affinity to F-Actin in Cells. We transfected HeLa cells with GFP-conjugated WT and K255E ACTN4 constructs (21), and performed fluorescence recovery after photobleaching (FRAP) experiments (22–25). In brief, we photobleached ∼1-μm diameter spots of GFP-ACTN4 for 1 s, and acquired images every 2 s to monitor the time-dependent recovery of fluorescence in that region (Fig. 1*B*). FRAP curves provide a direct measure of the average time for ACTN4 to unbind and move from the bleached region (24–26). Here, unbinding is much slower than transport, and as such the fluorescence recovery can be represented by a single exponential $I(t) = C - A * \exp(-t/\tau)$, where τ is the time constant representing the time required to recover ($\tau = 1/K_{off}$), A is related to K_{on} and K_{off} (25), and C is the immobile fraction of bound GFP-ACTN4 that does not unbind on the timescale of measurement (2 min) (25, 26). We performed FRAP measurements on both WT and K255E GFP constructs and find that the K255E recovery times are approximately three times as long as the WT constructs (WT 29 ± 13; K255E: 86 ± 29 s). From the exponential fit, we also determine the immobile fraction, C. Again, two distinct populations emerge, with WT ACTN4 having a lower immobile fraction (0.17 ± 0.06) than K255E (0.53 ± 0.14). These data demonstrate that the K255E mutation has a profound increase on the binding affinity of ACTN4 to actin in cells. Values are quoted in mean ± SD.

ACTN4 Cross-Linking Reduces Intracellular Movement. To compare the effects of WT and K255E ACTN4 constructs, we used human fibroblast cell lines from four different individuals (two lines per genotype: homozygous WT and heterozygous K255E) (27).

To study the effects of ACTN4 cross-linking on the cytoplasmic environment, we measured the trajectories of endocytosed fluorescent microspheres (28). High-speed confocal imaging of these particles allows us to resolve their time-dependent transport within the cytoplasm. We calculated the mean squared displacement (MSD) of these particles, shown in Fig. 2, which is a combination of the local viscoelasticity and driving forces impinging upon the particles (29). At short times less than 0.1 s, beads in both WT and K255E cells display similar mobility within the cytoplasm. At longer timescales, this bead mobility diverges; beads within WT cells begin to appear diffusive-like and approach a slope of 0.82 after 0.69 ± 0.09s, as shown in Fig. 2. This transition to diffusive-like movement of beads in the K255E cells takes approximately three times longer: only after 2.21 ± 0.45 s do beads in K255E cells appear diffusive-like, and approach a slope of ∼0.48. This delayed transition from local fluctuations to diffusive-like mobility is consistent with previous rheology of reconstituted ACTN4-actin systems, which has shown that a viscoelastic transition from solid-like to fluid-like behavior is delayed by the increased binding affinity of K255E (6, 17, 18).

Increased ACTN4 Binding Affinity Increases Cell Area and Slows Down Cell Migration.

Cell area. To resolve how the K255E mutation affects cell structure and morphology, we examined the spread area of the WT and K255E cells with the same set of fibroblast cell lines. We find

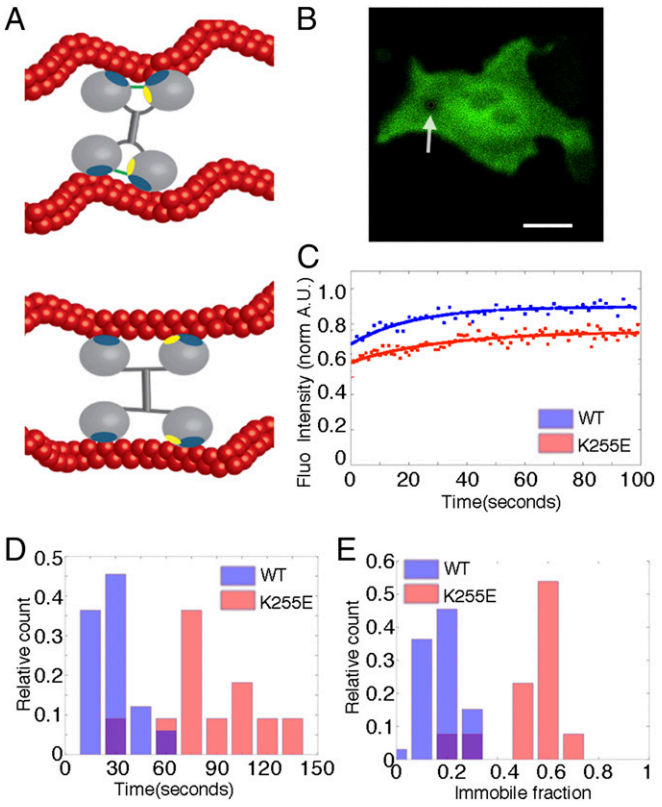

Fig. 1. ACTN4 binding face is altered in the K255E mutation. (*A*) Illustration of the binding interaction between WT (*Upper*) and K255E (*Lower*) ACTN4 with actin filaments. Principle actin binding domains are depicted in blue, with the third putative site in yellow. The K255E mutation removes the bridge (green top) allowing the third putative actin binding domain (yellow) to be exposed, which increases the cross-linker affinity for actin. (*B*) Representative FRAP experiment of photobleaching a local region of GFP-ACTN4. (Scale bar: 20 μm.) Cells are transfected to express GFP-conjugated WT or K255E ACTN4, and a 1-μm spot is photobleached within 1 s. The time-dependent recovery is monitored (*Supporting Information*). (*C*) Representative FRAP data collected from WT (blue) and K255E (red) GFP-conjugated ACTN4 constructs. Time-dependent fluorescence recovery of GFP-conjugated WT or K255E ACTN4 are monitored and then fit with a single exponential, $I(t) = C - A * \exp(-t/\tau)$. The time constant ($\tau$) of the exponential quantifies the average time required for the GFP-ACTN4 to dissociate from actin. (*D*) Histogram of time-constant exponents (τ) from fitting FRAP data. WT exponents are measured to be 29 ± 13 s, and K255E are 86 ± 29 s. (*E*) Histogram of immobile fraction, *C*, from fitting FRAP data. WT ACTN4 are measured to have a lower immobile fraction (0.17 ± 0.06), and K255E display a larger immobile fraction (0.53 ± 0.14). Values are quoted in mean ± SD.

that on average K255E cells spread to cover roughly twice as large an area as WT (WT ∼3,090 ± 981 μm^2; K255E: 5860 ± 326 μm^2), as shown in Fig. 3*B* (mean ± SD).

Cell migration. To measure how the change in ACTN4 affinity affects general cell migration, we monitored the trajectories of WT and K255E ACTN4 cells over 24 h. Reminiscent of the reduction in cytoplasmic mobility, we find that K255E-expressing cells are also less motile. Dividing the rms displacement of the movement of the centers of cellular area by the elapsed time, we find the speed of the K255E cells is significantly less than WT cells; over 24 h, WT cells move on average 1.16 ± 0.15 μm/h, and K255E cells move 0.55 ± 0.09 μm/h, as shown in Fig. 3*C* (mean ± SD).

Increased ACTN4 Binding Affinity Increases Contractile Forces, Strain Energy, and Persistence of Forces.

Contractile stresses. Due to the observed differences in cell spreading and motility between WT and K255E ACTN4 cells, we investigated

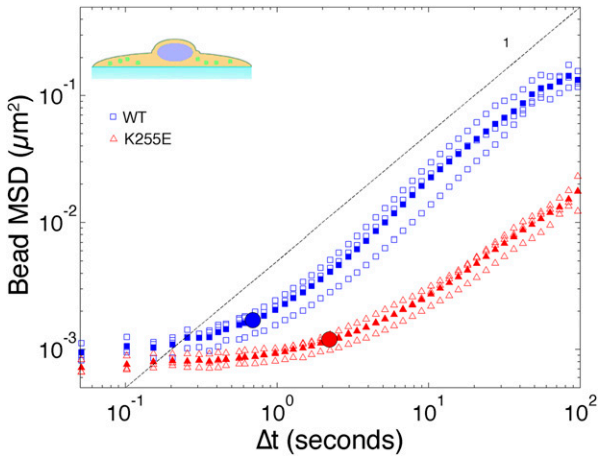

Fig. 2. The K255E mutation slows intracellular movement. Endocytosed 100-nm fluorescent particles are tracked in the fibroblast cell lines using confocal microscopy. The trajectories reveal the mobility of objects within the cytoplasm. MSD of the tracked particles is plotted as a function of time, demonstrating that particles in the WT (hollow blue square, solid squares are mean) cells are significantly more mobile than those in the K255E (hollow red triangles, solid triangles are mean) cells. At short times less than 0.1 s, beads in both WT and K255E cells display similar mobility within the cytoplasm; at longer timescales this bead mobility diverges; beads within WT cells begin to appear diffusive-like and approach a slope of 0.82 after 0.69 ± 0.09 s (blue circle). This transition to diffusive-like movement of beads in the K255E cells takes approximately three times longer; only after 2.21 ± 0.45 s (red circle) do beads in K255E cells appear diffusive-like and approach a slope of ∼0.48. The dashed black line provides a slope of unity as a guide. This delayed transition from local fluctuations to diffusive-like mobility in the K255E cytoplasm is consistent with previous rheology of reconstituted ACTN4-actin systems that has shown that a viscoelastic transition from solid-like to fluid-like behavior is delayed by the increased binding affinity of K255E.

differences in underlying contractile forces by plating cells on polyacrylamide (PAA) gels with embedded fluorescent tracer particles. We then used confocal microscopy to image the cell-induced deformations of the substrate, and calculated the cellular traction forces using traction force microscopy (TFM) (30). We then calculated the average magnitude of cell-exerted traction stresses using constrained Fourier transform traction cytometry traction force microscopy (30), as shown in Fig. 3*A*. These values can be represented as rms of traction stress, which reports the average local stress magnitude. When plated on 26-kPa PAA substrates, we found that cells with K255E ACTN4 have roughly threefold increased rms traction stresses (from 1.8 ± 0.7 to 4.7 ± 0.5 kPa), as shown in Fig. 3*D*.

To investigate the role of substrate stiffness in mediating these forces, we also plated WT and K255E cells on 4-kPa PAA substrates. We found that the rms traction of K255E cells to be again roughly three times larger than that of the WT cells, (77.26 ± 6.81 to 238.9 ± 50.21 Pa), as shown in *Supporting Information*. This comparison reveals that though the magnitude of traction stresses scales with substrate stiffness, the relative approximate threefold difference in traction stress is retained over different substrate moduli.

Strain energy. Though the contractile stress quantifies the local forces generated by adherent cells, it does not capture the total work done by the cells; in equilibrium between two nondissipative elastic materials, an arbitrary force may be retained without adding further energy to the system. Because we hypothesize that the principle difference between the WT and K255E ACTN4 constructs lies in the differential actin-binding affinity, and the resulting relaxation timescale of the actin network (4, 17), we examined changes in the total work done by the cell on the elastic substrate by measuring the total strain energy embodied in the substrate as a result of cell contraction as described previously (31).

We find that the strain energies on 26-kPa substrates are 2.1 ± 0.4 and 0.4 ± 0.23 pJ for the K255E and WT ACTN4 cells, respectively, representing a roughly fivefold increase in cell work done on the substrate due to the K255E mutation (Fig. 3*E*).

Persistence of contractile forces. Observing the traction force dynamics over a period of 24 h revealed that cells expressing K255E ACTN4 do not only exhibit larger traction forces, but that the local stresses generated are more persistent in time than those of WT ACTN4. To quantify this persistence of force, we examined the local hot spots of traction force, defined as being larger than 1 kPa, and tracked their duration over the course of 24 h (*Supporting Information*). The frequency of the average traction stress at these hotspots and their duration are shown in Fig. 4 *A* and *B*. Interestingly, both WT and K255E cell populations display a peak in their stress distribution at 1.2 kPa, but the WT displays a higher frequency at traction stresses less than about 1.4 kPa, and K255E displays increased frequency above 1.4 kPa. The difference between these distributions is shown in Fig. 4*A*, *Inset*. Complementarily, comparing the distribution of traction durations also reveals a peak shared between WT and K255E cells at brief durations less than 1 h, but the WT K255E cells display a clearly increased frequency at durations longer than roughly 4 h, extending well to 20 h. The difference between these distributions is shown in Fig. *4B*, *Inset*.

By merging traction force magnitude and persistence data, we create a 2D histogram of local traction stress and duration

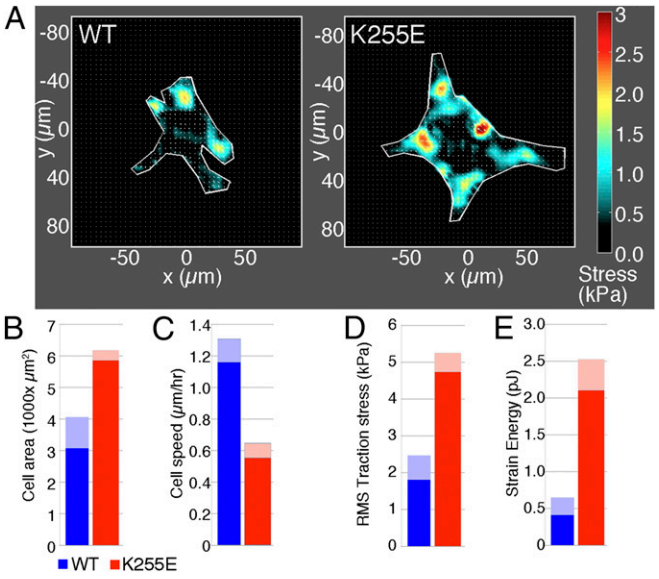

Fig. 3. Cells expressing K255E ACTN4 are more spread, slower, exert larger forces, and do more work than WT cells. (*A*) Representative traction force maps from WT (*Left*) and K255E (*Right*) cells calculated from 26-kPa polyacrylamide substrates. (*B*) Mean spread area of WT (blue) and K255E (red) cells. We find that, on average, K255E cells spread to cover roughly twice as large an area as WT (WT ∼3,090 ± 981 μm^2; K255E: 5,860 ± 326 μm^2; mean ± SD). (*C*) Mean speeds of WT (blue) and K255E (red) cells. We find the speed of the K255E cells is significantly less than WT cells; over 24 h, WT cells move on average 1.16 ± 0.15 μm/h, and K255E cells move 0.55 ± 0.09 μm/h (mean ± SD). (*D*) Mean rms traction stresses of WT (blue) and K255E (red) cells. We measure that WT ACTN4 cells exerted traction stresses of 1.8 ± 0.7 kPa, whereas K255E ACTN4 cells exert 4.7 ± 0.5 kPa. (*E*) Mean strain energy of WT (blue) and K255E (red). The strain energy measures the total elastic energy stored in the substrate, and is a measure of work done by the cell on the substrate. We measure that WT ACTN4 cells exert a strain energy of 0.4 ± 0.23 pJ, whereas K255E ACTN4 cells exert 2.1 ± 0.4 pJ (values quoted in mean ± SD).

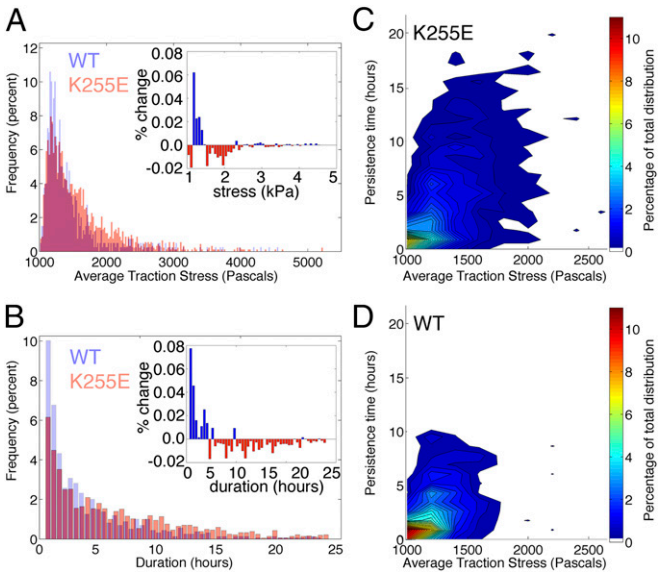

Fig. 4. K255E ACTN4 cells exert larger forces for longer durations. (*A*) Histogram of local traction stresses in WT (blue) and K255E (red). (*Inset*) Difference between distributions reveals that WT cells have a larger number of traction forces at 1.2 kPa, but that K255E are more pronounced from 1.4 to 2.2 kPa. (*B*) Histogram of traction stress durations in WT (blue) and K255E (red). (*Inset*) Difference between distributions reveals that WT cells traction stresses are briefer than K255E, and that K255E stresses are significantly more likely to last longer than 5 h. (*C*) 2D histogram of persistence of traction vs. traction force in K255E-expressing cells. The main locus of persistent forces is found at ∼50 min and 1 kPa, yet the distribution extends beyond 2 kPa and 15 h. (*D*) 2D histogram of persistence of traction vs. traction force in WT expressing cells. The main locus of persistent forces is found at ∼50 min and 1 kPa, and the distribution extends to ∼1.7 kPa and 10 h.

distributions, as shown in Fig. 4 *C* and *D*. Both K255E and WT cells display a locus of traction stress at ∼50 min duration and 1 kPa; however, the duration of K255E cell traction stresses extends ∼50% longer (from 10 to 15 h) and includes larger traction forces. The increased frequency of larger and more persistent traction forces in the K255E cells is consistent with the increase in measured strain energy compared with WT cells, and highlights the importance of time-dependent traction stress measurements in characterizing biophysical changes in the cytoskeleton.

Discussion

Here we have shown that increased cross-linker binding affinity to actin decreases cytoplasmic mobility and cellular movement, while increasing the contractile work done by cells. We propose that this counterintuitive result of increased forces yet decreased motility may be understood by examining the role of cross-linking in integrating contractile work done by molecular motors.

Cells, tissues, and organisms are not simply passively viscoelastic, but are indeed themselves active materials: within the actin cytoskeleton, myosin II pulls actin filaments generating tension and contractility. As assemblies of myosin motors contract and pull actin filaments, these forces either generate tension in the actin filaments, or cause them to slide, depending on the filaments' resistance to sliding: strongly cross-linked filaments resist sliding, and accumulate tension, whereas weakly cross-linked filaments slide more readily (4, 6, 11, 17).

We hypothesize that the cross-linker dissociation time may partition the work done by myosin between generating tension in the network (long τ = cross-linked filaments, solid-like behavior) and filament movement (short τ = sliding filaments, fluid-like behavior) (17). On average, at timescales shorter than τ, the cross-linkers remain bound and the filaments are interconnected, whereas at longer times the cross-linkers will unbind, allowing filaments to slide past each other (4). When filaments are cross-linked, myosin contractility is converted into tension, and the stress in the network increases; when filaments are not cross-linked, contractility is converted into filament movement (32).

Thus, the stronger cross-linking of K255E may prevent movement of actin filament sliding, thus reducing cell motility and cytoplasmic mobility, while simultaneously increasing tension in the actin network. This tension manifests in increased traction forces being applied to the substrate and increased cell spreading. The fact that the heterozygous K255E cell lines display such pronounced physical differences suggests that this mutation produces a biologically dominant phenotype.

We believe that the relationship between cross-linking and movement is likely biphasic; excessively prolonged cross-linking produces overly static structures, as previously proven in reconstituted systems and shown here with K255E ACTN4, whereas too brief or entirely absent cross-linking may create overly dissipative actin networks incapable of transducing sufficient force to migrate. Our results show that K255E-increased cross-linking reduces cell movement, but suggest that reducing or inhibiting cross-linking would reduce traction stress. This loss-of-traction stress could potentially prevent cells from migrating through crowded environments, providing an explanation for previous measurements of defective motility and adhesion without ACTN4 (33, 34). Thus, there may be an ideal range of cross-linking affinity for retaining mechanical integrity and force production, while permitting dynamic solidification to allow movement.

These principles also suggest how pathology may arise from mechanically disruptive single-point mutations in cytoskeletal proteins. Many tissues and organs appear to regulate their stiffness in proportion to the forces encountered in their environment, such that regions of low stress may be softer than those under high stress (35, 36); this may promote a "strain homeostasis," regulating the deformation of tissue to preserve the dynamic range of strain-dependent mechanobiology (26, 37, 38) or its mechanical sensitivity (39). We hypothesize that the physical changes related to the K255E ACTN4 mutation may be key in human kidney disease; the kidney is a pressure-driven filter, with separation of urine from blood occurring in microscopic spherically shaped bundles of capillaries (glomeruli) surrounded by interdigitating cells known as podocytes. Under peristaltic blood flow, these glomerular capillaries experience cyclic stress. We speculate that the K255E mutation may cause cellular structures to become excessively solid, and reduce the ability of the podocytes and glomeruli to flex and dissipate stress, causing a failure of this filtration barrier. This mechanism is consistent with the loss of normal "foot process" architecture observed in vivo in human kidney disease (13–15).

Given the central role of the actin cytoskeleton, disruption of the cell's mechanical properties through changes in actin cross-linker binding affinity may be related to a broad range of medical disorders linked to mechanical stress (40), from cardiac failure to pulmonary injury. Future work will define the role of these mechanical changes in kidney failure, as well as broader mechanobiology pathology.

Materials and Methods

Cell Culture. Four cell lines were generated from dermal fibroblasts and telomerase reverse transcriptase (TERT)-immortalized as described previously (27). Two independent cell lines were created from two individuals heterozygous for K255E mutations, and two lines from two individuals homozygous for the WT form of ACTN4. Generation of cell lines was performed in accordance with a protocol approved by the Institutional Review Board at Beth Israel Deaconess Medical Center. All cell lines were used to minimize potential artifacts from phenomena specific to a single cell line. Cells were cultured in DMEM supplemented with 10% (vol/vol) FCS, 100 U/mL penicillin, and 100 μg/mL streptomycin and maintained under 5% CO_2 at 37 °C in a humidified incubator. These cell lines were used in all experiments, aside

from fluorescence recovery after photobleaching (FRAP) studies, where HeLa cells were used.

FRAP Measurements of Binding Kinetics. GFP-conjugated constructs of WT and K255E ACTN4 were a gift from Carol Otey, University of North Carolina, Chapel Hill, NC (21). These plasmids were transfected into HeLa cells with Lipofectamine 2000 (Invitrogen) as per manufacturer's instructions. Transfected cells were locally bleached for 1 s using the FRAP module within confocal software (Leica SP5), and monitored for 2 min, acquiring an image every 2 s. Imaging settings were selected to minimize any additional photobleaching during acquisition, and all settings were kept constant over all experiments. In postprocessing using MatLab, data were normalized to the prebleach region-of-interest (ROI) intensities, and the recovery curve was normalized by a control ROI that monitored sample bleaching due to imaging. A single exponential, $I(t) = C - A * \exp(-t/\tau)$, was used to fit the intensity recovery in time, with the time-constant reported as τ, and the immobile fraction as C (24).

Tracking Endocytosed Particle Movements. Cells were passaged onto collagen I (PureCol; Advanced BioMatrix)-coated coverslips affixed to the bottom of cell culture dishes and allowed to grow overnight. To monitor intracellular movement, we tracked the motion of endocytosed 100-nm polystyrene fluorescent microspheres (Invitrogen). Particles were added 6 h before experimentation at a concentration to achieve ~20 particles per cell. The particles were visualized by confocal microscopy using a 63× 1.2 N.A. water-immersion lens on a Leica TSC SP5 microscope. Particles were confirmed to be in the cell interior rather than on the cell or substrate surface by examination in 3D space with confocal microscopy. To avoid complications from cell-boundary effects, only particles located away from the thin outer lamellar region and the nucleus were analyzed, to avoid interactions with the nucleus or artifacts from extracellular mechanics. The positions of the particles were recorded every 18 ms for 2 min. Particle centers were determined by finding the centroid of the particle's brightness in each image with an accuracy of 20 nm. Particle trajectories were tracked to calculate the time and ensemble-averaged MSD, $<\Delta r^2(\tau)>$, where $\Delta r(\tau) = r(t + \tau) - r(t)$ (28).

Traction Force Microscopy Measurements. The active cell contractile forces were measured using TFM as described previously (30). Briefly, cells were cultured on elastic PAA hydrogels of known compliance, with embedded fluorescent microspheres. For all traction force experiments, cells were plated on gels with a Young's modulus of ~26 kPa, except for the substrate stiffness comparison where 4-kPa substrates were used. Cell contractility-induced deformations of the substrate were measured by confocally imaging the bead positions with cells present. Cells were then removed with a detachment solution (3% Triton-X, 200 mM KOH, 0.5% NaAz), and the cell strain-free bead positions were measured. By knowing the substrate stiffness and measuring the local bead displacements, the active cell stresses on the substrate were calculated. Time-lapse traction measurements were performed in sealed dishes with CO_2-independent culture media (Invitrogen) in place of DMEM. Confocal images of cells and the substrate beads were captured every 10 min using a 10× air objective at 100 nm/pixel resolution.

Traction Force Persistence. To quantify this persistence of force, we examined the local hotspots of traction force, defined as being larger than some threshold (here, 1 kPa), and tracked their duration over the course of 24 h (*Supporting Information*). Artifacts of "blinking" hotspots (where tracking errors may incorrectly report a spot or its disappearance) are ameliorated by rejecting single time-point data. Thus, a hotspot period may not be shorter than two frames (20 min).

Calculation of Cell-Traction Stress and Strain Energy. Cell tractions were computed using constrained Fourier transform traction microscopy (FTTM) (31). Briefly, the displacement field was computed by comparing fluorescent microbead images obtained during the experiment with a reference image obtained at the end of the experiment subsequent to detaching the cell from its underlying substrate. The projected cell area was calculated based on a manual trace of the cell contour determined from a fluorescence image of the cell (CellTracker; Invitrogen) obtained every 10 min. From the displacement field we calculated the traction stress, described previously (31). To quantify the total work done on the substrate, we calculate the strain energy using the following equation (31):

$$U = \left(\frac{1}{2}\right) \int \vec{T}(\vec{r}) \cdot \vec{u}(\vec{r}) dxdy,$$

where U is the total strain energy, T is the traction at distance r, and u is the displacement at distance r.

Tracking Cell Movement. To monitor cell movement, we track cells labeled with a cell-permeable fluorescent dye (CellTracker; Invitrogen). These cells were imaged with confocal microscopy using a 10× 0.3 N.A. air objective. Cell centroids were determined by finding the center of the fluorescent cells. Centroids were tracked to calculate the individual and ensemble-averaged MSD, $<\Delta r^2(\tau)>$, where $\Delta r(\tau) = r(t + \tau) - r(t)$.

ACKNOWLEDGMENTS. The authors thank Ye Tian for technical assistance, Hossein K. Heris for helpful discussions, and Katherine Ehrlicher for technical illustration. This work was supported by NIH Grant PO1GM096971, the Harvard Materials Research Science and Engineering Center (DMR-0820484), and National Science Foundation Grant DMR-1310266. Additional support was provided by NIH Grants DK083592 and DK59588 (to M.R.P. and A.J.E.) and Natural Sciences and Engineering Research Council (NSERC) Discovery Grant 05843 (to A.J.E.).

1. Lieleg O, Schmoller KM, Claessens MM, Bausch AR (2009) Cytoskeletal polymer networks: Viscoelastic properties are determined by the microscopic interaction potential of cross-links. *Biophys J* 96(11):4725–4732.
2. Schmoller KM, Lieleg O, Bausch AR (2009) Structural and viscoelastic properties of actin/filamin networks: Cross-linked versus bundled networks. *Biophys J* 97(1):83–89.
3. Stamenović D (2006) Cell mechanics: Two regimes, maybe three? *Nat Mater* 5(8): 597–598.
4. Wachsstock DH, Schwarz WH, Pollard TD (1994) Cross-linker dynamics determine the mechanical properties of actin gels. *Biophys J* 66(3 Pt 1):801–809.
5. Janmey PA, Hvidt S, Lamb J, Stossel TP (1990) Resemblance of actin-binding protein/actin gels to covalently cross-linked networks. *Nature* 345(6270):89–92.
6. Ward SM, Weins A, Pollak MR, Weitz DA (2008) Dynamic viscoelasticity of actin cross-linked with wild-type and disease-causing mutant alpha-actinin-4. *Biophys J* 95(10): 4915–4923.
7. Blanchoin L, Boujemaa-Paterski R, Sykes C, Plastino J (2014) Actin dynamics, architecture, and mechanics in cell motility. *Physiol Rev* 94(1):235–263.
8. Fabry B, et al. (2001) Scaling the microrheology of living cells. *Phys Rev Lett* 87(14):148102.
9. Trepat X, et al. (2007) Universal physical responses to stretch in the living cell. *Nature* 447(7144):592–595.
10. Tang J, Taylor DW, Taylor KA (2001) The three-dimensional structure of alpha-actinin obtained by cryoelectron microscopy suggests a model for Ca(2+)-dependent actin binding. *J Mol Biol* 310(4):845–858.
11. Weins A, et al. (2007) Disease-associated mutant alpha-actinin-4 reveals a mechanism for regulating its F-actin-binding affinity. *Proc Natl Acad Sci USA* 104(41):16080–16085.
12. Otey CA, Carpen O (2004) Alpha-actinin revisited: A fresh look at an old player. *Cell Motil Cytoskeleton* 58(2):104–111.
13. Henderson JM, Alexander MP, Pollak MR (2009) Patients with ACTN4 mutations demonstrate distinctive features of glomerular injury. *J Am Soc Nephrol* 20(5):961–968.
14. Weins A, et al. (2005) Mutational and biological analysis of alpha-actinin-4 in focal segmental glomerulosclerosis. *J Am Soc Nephrol* 16(12):3694–3701.
15. Kaplan JM, et al. (2000) Mutations in ACTN4, encoding alpha-actinin-4, cause familial focal segmental glomerulosclerosis. *Nat Genet* 24(3):251–256.
16. Yao NY, et al. (2013) Stress-enhanced gelation: A dynamic nonlinearity of elasticity. *Phys Rev Lett* 110(1):018103.
17. Yao NY, et al. (2011) Nonlinear viscoelasticity of actin transiently cross-linked with mutant α-actinin-4. *J Mol Biol* 411(5):1062–1071.
18. Broedersz CP, et al. (2010) Cross-link-governed dynamics of biopolymer networks. *Phys Rev Lett* 105(23):238101.
19. Lieleg O, Claessens MMAE, Bausch AR (2010) Structure and dynamics of cross-linked actin networks. *Soft Matter* 6(2):218–225.
20. Wyss HM, et al. (2011) Biophysical properties of normal and diseased renal glomeruli. *Am J Physiol Cell Physiol* 300(3):C397–C405.
21. Edlund M, Lotano MA, Otey CA (2001) Dynamics of alpha-actinin in focal adhesions and stress fibers visualized with alpha-actinin-green fluorescent protein. *Cell Motil Cytoskeleton* 48(3):190–200.
22. Ishikawa-Ankerhold HC, Ankerhold R, Drummen GP (2012) Advanced fluorescence microscopy techniques—FRAP, FLIP, FLAP, FRET and FLIM. *Molecules* 17(4):4047–4132.
23. Lambert NA (2009) Uncoupling diffusion and binding in FRAP experiments. *Nat Methods* 6(3):183. author reply 183–184.
24. Sprague BL, McNally JG (2005) FRAP analysis of binding: Proper and fitting. *Trends Cell Biol* 15(2):84–91.
25. Sprague BL, Pego RL, Stavreva DA, McNally JG (2004) Analysis of binding reactions by fluorescence recovery after photobleaching. *Biophys J* 86(6):3473–3495.
26. Ehrlicher AJ, Nakamura F, Hartwig JH, Weitz DA, Stossel TP (2011) Mechanical strain in actin networks regulates FilGAP and integrin binding to filamin A. *Nature* 478(7368):260–263.

27. Rheinwald JG, et al. (2002) A two-stage, p16(INK4A)- and p53-dependent keratinocyte senescence mechanism that limits replicative potential independent of telomere status. *Mol Cell Biol* 22(14):5157–5172.
28. Guo M, et al. (2013) The role of vimentin intermediate filaments in cortical and cytoplasmic mechanics. *Biophys J* 105(7):1562–1568.
29. Guo M, et al. (2014) Probing the stochastic, motor-driven properties of the cytoplasm using force spectrum microscopy. *Cell* 158(4):822–832.
30. Krishnan R, et al. (2009) Reinforcement versus fluidization in cytoskeletal mechanoresponsiveness. *PLoS ONE* 4(5):e5486.
31. Butler JP, Tolić-Nørrelykke IM, Fabry B, Fredberg JJ (2002) Traction fields, moments, and strain energy that cells exert on their surroundings. *Am J Physiol Cell Physiol* 282(3):C595–C605.
32. Humphrey D, Duggan C, Saha D, Smith D, Käs J (2002) Active fluidization of polymer networks through molecular motors. *Nature* 416(6879):413–416.
33. Shao H, Wang JHC, Pollak MR, Wells A (2010) α-actinin-4 is essential for maintaining the spreading, motility and contractility of fibroblasts. *PLoS ONE* 5(11):e13921.
34. Honda K, et al. (2005) Actinin-4 increases cell motility and promotes lymph node metastasis of colorectal cancer. *Gastroenterology* 128(1):51–62.
35. Swift J, et al. (2013) Nuclear lamin-A scales with tissue stiffness and enhances matrix-directed differentiation. *Science* 341(6149):1240104.
36. Discher DE, Janmey P, Wang YL (2005) Tissue cells feel and respond to the stiffness of their substrate. *Science* 310(5751):1139–1143.
37. Krüger M, Linke WA (2009) Titin-based mechanical signalling in normal and failing myocardium. *J Mol Cell Cardiol* 46(4):490–498.
38. Moore SW, Roca-Cusachs P, Sheetz MP (2010) Stretchy proteins on stretchy substrates: The important elements of integrin-mediated rigidity sensing. *Dev Cell* 19(2):194–206.
39. Wang N, Tytell JD, Ingber DE (2009) Mechanotransduction at a distance: Mechanically coupling the extracellular matrix with the nucleus. *Nat Rev Mol Cell Biol* 10(1):75–82.
40. Ingber DE (2003) Mechanobiology and diseases of mechanotransduction. *Ann Med* 35(8):564–577.